Characterization of spin-orbit autoionizing Rydberg states excited via one-photon absorption from the F 1D2 Rydberg state of HBr.

Wales, N.P.L.; Buma, W.J.; de Lange, C.A.; Lefebvre-Brion, H.

DOI
10.1063/1.472171

Publication date
1996

Published in
Journal of Chemical Physics

Characterization of spin–orbit autoionizing Rydberg states excited via one-photon absorption from the $F\ ^1\Delta_2$ Rydberg state of HBr

N. P. L. Wales, W. J. Buma, and C. A. de Lange
Laboratory for Physical Chemistry, University of Amsterdam, Nieuwe Achtergracht 127, 1018 WS Amsterdam, The Netherlands

H. Lefebvre-Brion
Laboratoire de Photophysique Moléculaire, Bât. 213, Université de Paris-Sud, 91405 Orsay Cedex, France

(Received 18 April 1996; accepted 17 May 1996)

Rotationally and parity resolved excitation spectra of autoionizing Rydberg states of HBr in the energy region between the $^2\Pi_{3/2}$ and $^2\Pi_{1/2}$ ionic thresholds have been obtained in a double resonant excitation scheme via single rotational levels of the vibrationless $F\ ^1\Delta_2$ Rydberg state. A cursory examination of these spectra reveals the presence of s, p, d, and f Rydberg series. Apart from the f series, which show almost Hund's case (e) coupling, these series clearly exhibit an angular momentum coupling scheme intermediate between Hund's case (c) and (e). As a result it is difficult to assign them as converging upon specific ionic rotational thresholds. A detailed analysis of the excitation spectra has consequently been performed employing multichannel quantum defect theory calculations, allowing for a determination of the quantum defects of the Hund's case (a) basis states and the relevant transition moments, and, concurrently, the assignment of nearly all the observed autoionizing resonances. © *1996 American Institute of Physics.* [S0021-9606(96)03132-7]

I. INTRODUCTION

The presence of states with excitation energies exceeding the lowest rovibronic ionization energy is one of the dominant factors determining the final state distribution in a photoionization process. Coupling of these states with the ionization continua of lower lying ionic states provides for a finite ionization probability of such states and results in autoionization, in which the excited ionic core undergoes energy relaxation and an electron is ejected. In atoms this energy relaxation process of the ionic core is per se electronic in nature, in molecules vibrational and rotational degrees of freedom become also available.

In molecules a detailed elucidation of the spectroscopic and dynamic properties of autoionizing Rydberg states requires excitation spectra with rotational resolution. In the majority of cases studied as yet this has not proved possible: either the coupling with underlying ionization continua is relatively strong and results in lifetime broadening and concurrent loss of resolution, or other decay channels such as (pre)dissociation are dominantly present. In this context, hydrogen halides have proven to be a particularly attractive class of molecules.[1–4] Here, the Rydberg states converging upon the $^2\Pi_{1/2}$ spin–orbit excited rovibronic ionic thresholds are subject to autoionization, but still have a width which is relatively small compared to rotational spacings, and therefore exhibit rotationally resolved excitation spectra.

The Rydberg states of hydrogen halides converging upon the ground ionic state possess a $^2\Pi$ ionic core. Spin–orbit interaction in these states derives primarily from the ionic core. There are consequently two sets of Rydberg states: one converging upon the $^2\Pi_{3/2}$ and the other upon the $^2\Pi_{1/2}$ ionic state. For low values of the principal quantum number n these states are described in Hund's case (c).[5] However, as the Rydberg electron is excited to orbits with larger principal quantum numbers, its movement becomes decoupled from the internuclear axis. In this situation the core is free to rotate as the ionic state to which the Rydberg state converges, and Hund's case (c) is no longer the appropriate coupling scheme. Instead, Hund's case (e) is approached.[6,7] In this limit J^+ and Ω^+ as well as the parity of Λ doublet components of the ion core are well defined. The angular momentum of the Rydberg electron is specified, $j=l+s$, but its projection, ω, on the molecular axis is no longer a good quantum number.

The uncoupling of j that accompanies the transition from Hund's case (c) to (e) has been the focus of several studies employing extensive use of multichannel quantum defect theory (MQDT) calculations.[2–4] In HI[2] the lowest autoionizing Rydberg levels are at $n=5$, placing them in Hund's case (c). As n increases an intermediate coupling scheme between Hund's case (c) and (e) was required for a proper description. Experiments have also been extended to HCl, either by vuv one-photon or double-resonant MPI techniques.[1,3,4] Despite the availability of accurate data on ionization thresholds, an unambiguous assignment was inhibited as a result of the congested spectrum obtained between the spin–orbit ionic states arising from the high density of states in this region. The lowest autoionizing Rydberg state starts here at $n=14$ and, as a consequence, considerable overlap occurs between the various Rydberg series.

In the present study we focus our attention on the autoionizing Rydberg states of the hydrogen halide HBr between its $^2\Pi_{3/2}$ and $^2\Pi_{1/2}$ ionic states. Here, the spin–orbit coupling in the $^2\Pi$ ionic state ($\approx$2600 cm^{-1}) is considerably larger than in HCl and allows for the study of states with principal quantum numbers, n, as low as 7. The density of autoionizing states near the $^2\Pi_{3/2}$ threshold is thus considerably lower than in HCl, and less crowded excitation spectra

 0021-9606/96/105(8)/2978/14/$10.00

are expected. Equally important is the observation that ZEKE-PFI studies performed in our group[8] and by others[9] have provided for quite accurate absolute rotational ionic thresholds, thereby making a unique assignment of observed resonances feasible.

In our experiments autoionizing Rydberg states have been excited in a two-color $(2+1')$ excitation process via the $F\ ^1\Delta_2\ 5p\pi$ Rydberg state. The first step, two-photon excitation of the $F\ ^1\Delta_2$ state, selects one particular rotational level of well-defined parity in this intermediate state, whose quantities will be labeled in the following with double primes. The subsequent excitation step is subject to the usual one-photon excitation angular momentum constraints $(\Delta J = J' - J'' = 0, \pm 1)$ and will therefore excite only a limited number of final states. The resulting excitation spectra will be analyzed and assigned by means of MQDT calculations. These assignments will derive further support from a comparison with the results of a study in which autoionizing states have been excited by one-photon vuv excitation from the ground state.[10]

II. EXPERIMENT

The experimental setup has been described before,[8] and will only briefly be discussed here. The spin–orbit autoionization spectra of HBr were recorded in a ''magnetic bottle'' time-of-flight electron spectrometer. In the ionization chamber of this spectrometer two grids are mounted on the magnetic pole faces which are employed for the application of static and/or pulsed electric fields. In the present experiments a small negative static field (−2 V/cm) was used in order to increase the collection efficiency for the slow electrons arising from the autoionization process. Excitation spectra were obtained by monitoring the yield of these slow photoelectrons as a function of the total excitation energy.

The laser system consists of a Lumonics HyperEX 460 excimer laser pumping two Lumonics dye lasers (HD500 and HD300). The output of the first dye laser (HD500), operating on Coumarin 500, was frequency doubled (Lumonics HyperTrak 1000) using a BBO crystal. The resulting uv light was focused into the ionization region by a quartz lens (focal length 25 mm) and used to drive various two-photon transitions to the $F\ ^1\Delta_2$ Rydberg state of HBr. The fundamental output of the second dye laser, operating on Rhodamine 6G, Coumarin 540, or Coumarin 500, was focused by a separate lens on the opposite side of the spectrometer and scanned over the region between the $^2\Pi_{3/2}$ and $^2\Pi_{1/2}$ ionic states. In our experiments it was found that the one-photon transitions from the $F\ ^1\Delta_2$ Rydberg state to the various autoionizing states could easily be saturated. The output of the probe laser was consequently attenuated to such an extent that saturation was avoided, as evidenced by the observation that the intensity of the autoionizing resonances was proportional to the intensity of the probe laser. Both laser pulses were overlapped in time using a fast silicon photodiode (HP5082) and intersected an effusive beam of pure HBr (Messer Griesheim 2.8, 99.8%) at right angles.

The probe laser was calibrated using known transitions of neon excited in a hollow cathode discharge.[11] The pump laser (HD500) was calibrated against well-known HBr (2+1) REMPI resonances.[12] The accuracy of the three-photon energies is estimated to be 0.5 cm^{-1}.

The excitation spectra to be discussed span the dye gain curves of three dyes. The spectra have not been corrected for their respective dye gain curve, though they have been partially intensity normalized in going from one dye to another by utilizing the overlap in the gain curves.

III. RESULTS AND DISCUSSION

A. Excitation spectra

Figures 1 and 2 show double-resonant excitation spectra of HBr in the energy region between the $^2\Pi_{3/2}$ and $^2\Pi_{1/2}$ spin–orbit components of its lowest ionic state obtained after two-photon excitation of the $J''=2$ rotational level of the $F\ ^1\Delta_2$ $(v''=0)$ Rydberg state via the $S(0)$ and $R(1)$ transitions, respectively. Excitation via $S(0)$ prepares the positive component of this particular level in the intermediate state, whereas the $R(1)$ transition populates the negative component. The spectra show well-defined series of autoionizing Rydberg states converging upon the various rotational levels of the $^2\Pi_{1/2}$ ionic state.

The $F\ ^1\Delta_2$ Rydberg state of HBr has previously been shown to be unperturbed.[8] Our recent REMPI-PES studies have demonstrated that photoionization of the $F\ ^1\Delta_2$ $(v''=0)$ level occurs exclusively to the vibrationless level of the $^2\Pi_{1/2}$ spin–orbit component of the ion. We can consequently safely conclude that the observed autoionizing Rydberg states in Figs. 1 and 2 converge solely upon rotational levels of the ground vibrational level of the $^2\Pi_{1/2}$ ionic state. Rydberg states converging upon higher rotational thresholds of the $^2\Pi_{3/2}$ spin–orbit component or higher vibrational thresholds of the two $^2\Pi$ components as has been observed in one-photon vuv studies from the ground state[13] are not excited. Moreover, on the basis of the angular momentum composition of the $5p\pi$ orbital of the $F\ ^1\Delta_2$ Rydberg state (96.57% p, 3.39% d, and 0.03% f),[14] one-photon transitions from this state would lead one to expect that s and d autoionizing Rydberg states should be dominant in the spectra. However, if the autoionizing Rydberg states are grouped into s and d quantum defect space, one immediately is forced to conclude that Rydberg series other than s and d are present with significant intensity in the spectra. Such a conclusion is *a posteriori* not so unexpected when the results of our previous ZEKE-PFI studies via the $F\ ^1\Delta_2$ Rydberg state[8] are considered. There it was observed that contributions from odd partial waves (p and f) were also present in the spectra, contributing up to 20% of the total ion population. The spectra shown in Figs. 1 and 2 have therefore been analyzed, not only in terms of s and d Rydberg series, but p and f Rydberg series as well. As will become clear later (*vide infra*), a detailed analysis of the excitation spectra on the basis of a search for series with constant quantum defects is not possible. Nevertheless, a rough indication of the identity of the resonances in terms of their being members of s, p, d, or f series can be obtained by assuming that they are grouped

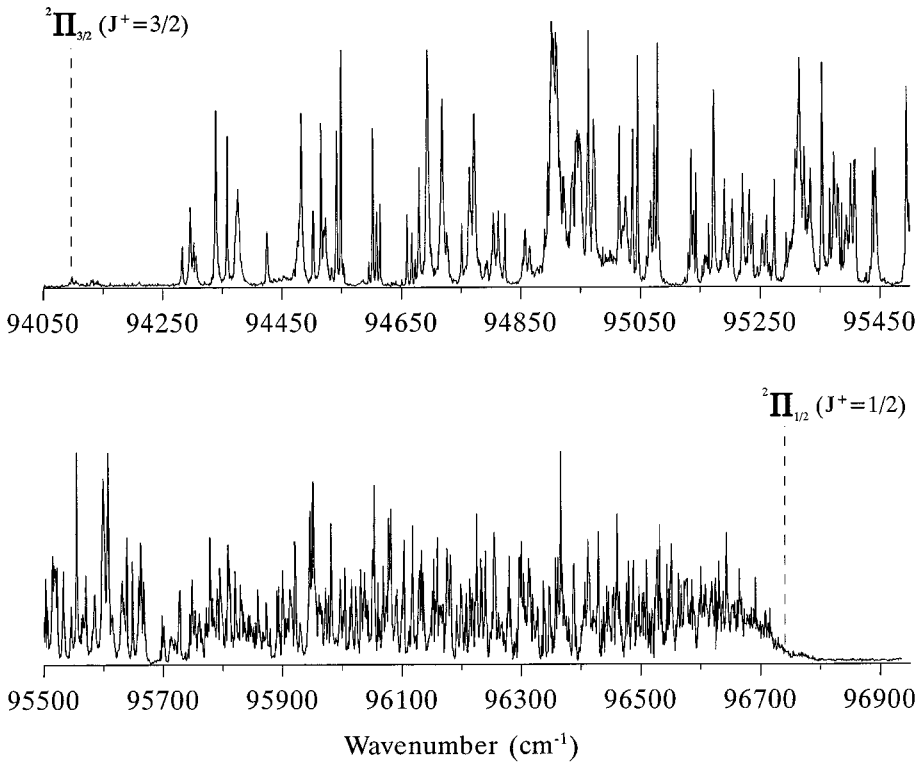

FIG. 1. Spin–orbit autoionization spectrum of HBr via the $S(0)$ rotational transition to the $F\ ^1\Delta_2$ ($v''=0$) Rydberg state.

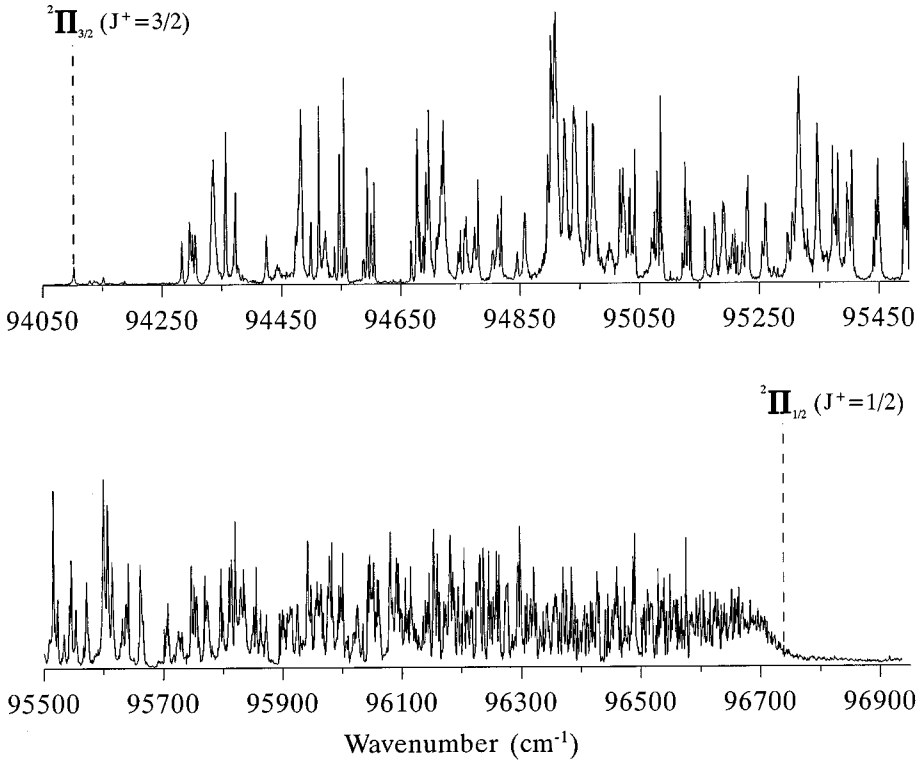

FIG. 2. Spin–orbit autoionization spectrum of HBr via the $R(1)$ rotational transition to the $F\ ^1\Delta_2$ ($v''=0$) Rydberg state.

approximately at quantum defects (modulo 1) of 0.1, 0.6, 0.3, and 0.0, respectively, with respect to the various rotational ionic thresholds. Furthermore, each resonance is characterized by its width, shape, and intensity. With this in mind we are able to isolate groups of resonances belonging to one of the above mentioned series.

Since the initial $S(0)$ two-photon transition populates the positive parity component of the $J''=2$ rotational level of the $F\ ^1\Delta_2$ state, only negative parity final Rydberg states can be excited at the three-photon level. The parity of these states is a product of the parity of the ionic rotational level to which the Rydberg state converges, and the parity of the angular momentum of the Rydberg electron. Since the parity of the Rydberg electron is given by $(-1)^l$, l being the electron's angular momentum, *s* and *d* electrons have positive parity, whereas *p* and *f* electrons have negative parity. This implies that *s* and *d* Rydberg states, populated via the $S(0)$ transition, converge to *negative* parity ionic rotational levels. The opposite is true for *p* and *f* Rydberg states. On the other hand, *s* and *d* Rydberg states populated via the $R(1)$ transition converge to *positive* parity ionic levels. Again the reverse is true for *p* and *f* states. We consequently can conclude that the final states reached via the $S(0)$ and $R(1)$ rotational transition have opposite parity. Since lambda doubling in the $^2\Pi_{1/2}$ ionic state is reasonably large,[15] we would expect that the excitation spectra of the autoionizing states obtained via the $S(0)$ and $R(1)$ transitions to the $F\ ^1\Delta_2$ state will exhibit significant differences with respect to peak positions and intensities. Such expectations are indeed well borne out in the spectra displayed in Figs. 1 and 2. This was also noted in a similar study of autoionizing Rydberg states of HCl accessed via the $D\ ^1\Pi_1$ Rydberg state.[3]

After one-photon absorption from the $F\ ^1\Delta_2\ J''=2$ state, Rydberg states are accessible with a total angular momentum J' of 1, 2, or 3. These transitions correspond to the *P*, *Q*, and *R* rotational branches in the autoionizing spectra, respectively. If the angular momentum of the Rydberg electron plus its spin in the final state is denoted as j, the accessible core rotational quantum numbers are defined by $|J'-j|\leqslant J^+\leqslant J'+j$. According to this selection rule the range of rotational quantum numbers of the ionic core is limited to $1/2\leqslant J^+\leqslant 7/2$ when exciting an autoionizing *s*-Rydberg state ($l=0$) and increases for larger values of l, e.g., for an *f*-Rydberg state ($l=3$) J^+ is restricted to $1/2\leqslant J^+\leqslant 13/2$. As a result of the large spin–orbit coupling in the $^2\Pi$ ionic state, the appropriate angular momentum coupling scheme of the final autoionizing states excited in our experiments is intermediate between Hund's case (c) and (e), and cannot be fully characterized in terms of J^+, which is only a good quantum number in Hund's case (e). In practice this means that for a given J' the final states excited via the *P*, *Q*, and *R* branches will not coincide. This splitting diminishes as n increases and finally disappears when Hund's case (e) becomes valid.

The *P*, *Q*, and *R* transitions from the $F\ ^1\Delta_2$ ($J''=2$) level will, in general, have different intensities. The fundamental reason for this is found in the contributions to their transition moments. If we consider for the moment the $F\ ^1\Delta_2$ state as a pure Hund's case (a) singlet state, Hund's case (a) selection rules ($\Delta\Lambda=0,\ \pm1,\ \Delta S=0,\ \Delta\Sigma=0$) would allow for three possible transitions, i.e., to $^1\Delta_2$, $^1\Pi_1$, and $^1\Phi_3$ states. In our specific case, i.e., transitions from the $J''=2$ level, the *P* transition is only possible to a $^1\Pi_1$ state, since the $J'=1$ level does not exist for $^1\Delta_2$ and $^1\Phi_3$ states. For analogous reasons the *Q* transition derives its intensity from the transition moments to $^1\Delta_2$ and $^1\Pi_1$ states, while the *R* transition has contributions from all three transition moments. In reality, the $F\ ^1\Delta_2$ state of HBr should be described in Hund's case (c) as a mixture of Hund's case (a) basis states: $F\ ^1\Delta_2=1/\sqrt{2}(^1\Delta_2+^3\Delta_2)$.[16] Transitions from the $^3\Delta_2$ part of this wave function are possible to $^3\Delta_2$, $^3\Pi_1$, and $^3\Phi_3$ states, and since the transition moments to these states are, to a first approximation, equal to their singlet counterparts,[17] the above conclusions concerning the possible *P*, *Q*, and *R* transitions will remain valid.

Consideration of the Hund's case (a) states that can be constructed from the $[^2\Pi_{1/2}]nl\lambda$ configurations[1] leads to the conclusion that for transitions to *d* and *f* autoionizing Rydberg states we may anticipate that *R* branch transitions will be more intense than *Q* branch transitions, which, in turn, will be more intense than *P* branch transitions. Similarly, for transitions to *p* autoionizing Rydberg states $R\approx Q>P$, while for *s* autoionizing Rydberg states all the branches should be approximately of the same intensity. It is clear that the above intensity ratios are only qualitative: The actual ratios are highly dependent on the size of the individual transition moments to the final Hund's case (a) states and the composition of the final states in terms of Hund's case (a) states.

In experiments carried out via higher J'' of the intermediate state (not shown) higher J' final states have been accessed. This has the effect of shifting the intensity in the spectrum to resonances that possess a larger ionic rotational quantum number, i.e., the intensity in the spectrum is shifted towards higher energies. Such autoionization spectra via higher J'' may serve as a useful guide to the analysis of spectra via lower J''. For example, $J'=1$ final states cannot be accessed via the $J''=3$ level of the intermediate state. Therefore, resonances that appear in the $S(0)$ or $R(1)$ spectra, but are not present when exciting via the $R(2)$ or $S(1)$ rotational transitions, can confidently be assigned to $J'=1$ states.

With the above considerations in mind, we have analyzed and assigned the autoionization spectra displayed in Figs. 1 and 2. The analysis of these spectra has been limited up to 95 700 cm^{-1}, corresponding to principal quantum numbers of $n=7$ to $n=10$. No attempt has been made to analyze the region beyond 95 700 cm^{-1} up to the $^2\Pi_{1/2}$ ionization limit, since the density of states in this region is such that a reliable assignment is no longer feasible. Below 95 700 cm^{-1} *s*, *p*, *d*, and *f* Rydberg series fall at well-isolated positions and only begin to merge at about $n=10$, thereby permitting a unique characterization of the states.

B. MQDT calculations

In the previous section we have argued that the Rydberg states in this part of the spectrum will exhibit an angular

TABLE I. Rotational thresholds of the $^2\Pi_{1/2}$ ionic state (Ref. 8).

Ionic rotational level	$^2\Pi_{1/2}$ thresholds (cm^{-1})
+1/2	96 741.6
−1/2	96 743.6
+3/2	96 768.6
−3/2	96 764.5
+5/2	96 803.4
−5/2	96 809.5
+7/2	96 866.2
−7/2	96 858.1
+9/2	96 928.8
−9/2	96 938.9
+11/2	97 027.5
−11/2	97 015.3
+13/2	97 117.6
−13/2	97 131.8
+15/2	97 251.9
−15/2	97 235.7

momentum coupling scheme which is intermediate between Hund's case (c) and (e) and will moreover change as a function of n. This implies that an analysis of the spectrum based on the identification of series with constant quantum defects is doomed to fail. Instead, it is necessary to model any situation intermediate between two coupling cases correctly. Although this can be accomplished via several approaches, the most convenient one and indeed our method of choice involves the use of MQDT calculations. For such calculations a number of parameters are required. These parameters concern the rotational ionic thresholds of the $^2\Pi_{1/2}$ state, the quantum defects of the possible Hund's case (a) basis states, and the transition moments from the $F\ ^1\Delta_2$ state to these states. Highly accurate spectroscopic constants of the $X\ ^2\Pi$ ionic state have previously been determined in a laser magnetic resonance study on the HBr^+ ion.[15] The absolute ionization energy of the $X\ ^2\Pi$ ionic system, on the other hand, has recently been obtained by our group in a ZEKE-PFI study via the $f\ ^3\Delta_2$ and $F\ ^1\Delta_2$ Rydberg states,[8] as well as by others in a vuv ZEKE-PFI study from the ground state.[10] Combination of these data yields the necessary accurate values of the rotational ionic thresholds,[8] which are given in Table I. As a starting point quantum defects have been employed that derive either from *ab initio* calculations,[13] Rydberg states of HBr with excitation energies below the lowest ionization limit,[12,18–20] or from analogous Rydberg states in HCl[3] and HI.[2] A number of these Rydberg states are best described in Hund's case (c) coupling. In order to obtain Hund's case (a) quantum defects, their excitation energies have been deperturbed from Hund's case (c) to case (a), allowing for the calculation of their quantum defects with respect to the $^2\Pi$ ionic limit, taken as the average of the $^2\Pi_{3/2}$ and $^2\Pi_{1/2}$ ionic thresholds. These initial values have been given in Table IV under the label of *ab initio* quantum defects. Finally, initial transition moments have been obtained from *ab initio* calculations.[16]

Under these assumptions excitation spectra have been calculated and subsequently fitted to the experimental spectra by iterative changes of the quantum defects such that no more improvement occurs. We note that such changes are not arbitrary since the quantum defects have a physical significance and are consequently restricted by particular rules, e.g., triplet states have larger quantum defects than their singlet counterparts. Once a satisfactory fit has been obtained with respect to *peak positions* of the resonances, further improvements in the comparison between the experimental and predicted spectra may be achieved by modification of the transition moments, which will change the *peak intensities* of the resonances. Manipulation of these intensities can also be accomplished to a certain extent by changing the difference between the quantum defects of the singlet and triplet states, since a large difference will broaden the resonance and lower its peak intensity. The assignments of these resonances in Figs. 1 and 2 to the various members of the s, p, d, and f Rydberg series are given in Tables II and III for excitation via $S(0)$ and $R(1)$, respectively. In these tables a comparison is made as well with the resonance positions as predicted from the MQDT calculations, based upon the fitted parameters reported in Tables IV and V. Since none of these Rydberg states can be described in pure Hund's case (e) coupling, it is, strictly speaking, not possible to assign a definite J^+ rotational quantum number to the resonances. Moreover, some lines are overlapped by smaller contributions from other Rydberg states. The assignments given in Tables II and III in terms of (J',J^+) therefore merely serve to indicate the state which has the largest contribution to a particular observed resonance. The autoionization spectra predicted by the MQDT calculations for $n=7$ and $n=8$ are displayed in Figs. 3 and 4, together with the experimentally observed spectra for excitation via $S(0)$ and $R(1)$, respectively.

Above we have noted that the $5p\pi$ Rydberg electron of the $F\ ^1\Delta_2$ state has predominantly p character. Transitions to s and d Rydberg states would, therefore, be expected to dominate the excitation spectra. This clearly does not bear out in the analysis. The s states are difficult to locate since they are in a spectral region where there is considerable overlap with the f states. The latter states are a dominant feature in the autoionization spectra (*vide infra*) and hence overshadow the unexpectedly weak s series. Very few lines are actually observed that arise from s states and some peaks predicted by the MQDT calculations are even missing. The s peaks that can be seen are quite broad at low n, but, as expected, narrow with increasing n. On the other hand, the d resonances are easily observed at well-defined positions. They are broad and very strong, especially those that converge upon higher J^+. As anticipated the majority of these lines arise from Q and R branch transitions.

The most surprising observation is the presence of rather intense p and f series in the spectra. The p-state resonances fall at well-isolated positions with some residual overlap with the d states, thereby allowing them to be readily identified. However, the p states seem to be perturbed and an unambiguous assignment is difficult. This is more evident for states that converge upon higher ionic rotational quantum numbers. Furthermore, the p series have an intensity which

TABLE II. Assignment of spin–orbit autoionizing Rydberg series via the $S(0)$ transition of the $F\ ^1\Delta_2$ Rydberg state of HBr together with results of corresponding MQDT calculations using the rotational ionic thresholds reported in Table I and the fitted parameters given in Tables IV and V.

	$S(0)$ $J''=2\ (+)$				
	E_{obs} (cm^{-1})	μ_{obs}	E_{theory} (cm^{-1})	μ_{theory}	Assignment[a] J',J^+
f-Rydberg complex[b]					
$n=7$					
	94 479.1	0.036	94 480.0	0.034	3,1/2
			94 482.1	0.031	2,1/2
	94 482.3	0.031	94 483.9	0.028	3,1/2
	94 502.5	0.041	94 503.9	0.039	2,3/2
	94 515.5	0.021	94 511.1	0.028	3,3/2
	94 541.5	0.035	94 539.1	0.038	2,5/2
	94 548.8	0.023	94 545.9	0.028	3,5/2
	94 595.1	0.049	94 599.5	0.042	1,7/2
	94 601.4	0.039	94 603.4	0.036	2&3,7/2
	94 607.8	0.029	94 606.1	0.032	2,7/2
	94 614.0	0.020	94 611.3	0.024	1&3,7/2
	94 659.1	0.047	94 662.5	0.041	1,9/2
	94 672.7	0.026	94 672.3	0.026	2,9/2
$n=8$					
	95 014.8	0.028	95 015.1	0.028	2&3,1/2
	95 036.8	0.040	95 037.3	0.039	2,3/2
	95 045.1	0.021	95 041.9	0.028	3,3/2
	95 073.4	0.036	95 072.3	0.038	2,5/2
	95 078.8	0.023	95 076.7	0.028	3,5/2
	95 130.7	0.048	95 133.5	0.042	1,7/2
	95 134.7	0.039	95 136.0	0.036	2&3,7/2
	95 139.2	0.029	95 137.7	0.032	2,7/2
$n=9$					
	95 143.1	0.020	95 141.3	0.024	3,7/2
	95 195.5	0.043	95 196.1	0.042	2,9/2
	Overlap with *p* state		95 198.3	0.037	1,9/2
			95 202.7	0.027	2,9/2
	95 380.1	0.022	95 378.5	0.028	2&3,1/2
	Overlap with *d* state				
	95 400.9	0.043	95 402.1	0.039	2,3/2
	95 407.9	0.020	95 405.5	0.028	3,3/2
	95 438.5	0.033	95 437.1	0.038	2,5/2
	95 442.1	0.022	95 440.1	0.028	3,5/2
	95 498.1	0.044	95 498.7	0.042	1,7/2
	95 502.9	0.028	95 500.7	0.035	2&3,7/2
			95 501.8	0.032	2,7/2
	95 504.2	0.024	95 504.2	0.024	3,7/2
	95 562.7	0.037	95 561.3	0.042	3,9/2
			95 562.7	0.037	1,9/2
	95 565.2	0.029	95 566.0	0.027	2,9/2
$n=10$					
	95 638.8	0.025	95 638.2	0.027	2&3,1/2
	95 662.5	0.040	95 662.8	0.038	2,3/2
	95 667.2	0.018	95 665.1	0.028	3,3/2
	95 698.1	0.036	95 697.7	0.038	2,5/2
	95 701.1	0.022	95 699.9	0.028	3,5/2
d-Rydberg complex					
$n=7$					
	94 296.2	0.332	94 297.5	0.331	3,3/2
	94 302.0	0.385	94 303.7	0.382	2,5/2
	94 338.8	0.336	94 334.6	0.341	3,5/2
	94 358.1	0.309	94 352.9	0.316	2,5/2
	94 375.6	0.351	94 375.0	0.352	3,7/2
	94 425.1	0.284	94 436.3	0.269	3,7/2
		0.393	94 436.3	0.378	3,9/2
$n=8$					
	94 679.1	0.709	94 677.4	0.712	1,1/2
	94 693.2	0.721	94 696.9	0.715	1,3/2

TABLE II. (*Continued.*)

	$S(0)$ $J''=2$ (+)				
	E_{obs} (cm^{-1})	μ_{obs}	E_{theory} (cm^{-1})	μ_{theory}	Assignment[a] J',J^+
	Overlap with p state				
	94 903.8	0.320	94 904.7	0.319	3,3/2
	94 909.7	0.400	94 912.2	0.395	2,5/2
	94 942.9	0.333	94 936.3	0.346	3,5/2
	94 963.0	0.390	94 963.5	0.389	2,7/2
	94 972.5	0.371	94 978.3	0.360	3,7/2
$n=9$					
	95 164.1	0.665	95 161.8	0.671	1,1/2
	95 189.1	0.654	95 180.4	0.677	1,3/2
	Overlap with p state				
	95 314.9	0.299	95 311.3	0.310	3,3/2
	95 322.5	0.409	95 323.3	0.407	2,5/2
	95 333.6	0.377	95 337.0	0.367	3,5/2
	95 353.3	0.319	95 347.7	0.336	3,5/2
	95 373.4	0.403	95 376.6	0.394	2,7/2
	95 380.0	0.384	95 386.1	0.366	3,7/2
	Overlap with f state				
$n=10$					
	95 498.1	0.613	95 497.0	0.618	1,1/2
	95 515.1	0.549	95 514.7	0.550	2,1/2
	95 555.1	0.474	95 555.5	0.473	3,3/2
	Overlap with p state				
	95 585.1	0.354	95 591.5	0.328	2,3/2
	95 599.3	0.295	95 598.7	0.298	3,3/2
	95 607.1	0.447	95 613.9	0.420	2,5/2
	95 621.2	0.390	95 615.1	0.415	3,5/2
	95 648.1	0.280	95 645.6	0.290	3,5/2
	Overlap with s state				
	95 669.8	0.390	95 669.2	0.393	2,7/2
p-Rydberg complex $n=8$					
	94 693.2	0.681	94 691.8	0.683	1,1/2
	Overlap with d state				
	94 717.8	0.636	94 717.2	0.637	1,1/2
	94 727.0	0.669	94 731.9	0.660	1,3/2
	94 751.1	0.625	94 750.8	0.625	1,3/2
	94 764.1	0.664	94 766.5	0.660	2,5/2
	94 772.0	0.650	94 781.0	0.634	2,5/2
	94 793.1	0.612	94 791.5	0.615	3,5/2
	94 824.1	0.669	94 827.0	0.664	2,7/2
	94 857.4	0.609	94 860.1	0.604	3,7/2
	Overlap with d state		94 907.1	0.633	3,9/2
$n=9$					
	95 157.1	0.678	95 157.1	0.678	1,1/2
	95 172.6	0.637	95 174.1	0.633	1,1/2
	95 190.1	0.662	95 190.9	0.660	1,3/2
	95 203.1	0.628	95 203.0	0.628	2,3/2
			95 206.5	0.619	1,3/2
	95 220.3	0.581	95 224.6	0.633	2,3/2
	95 231.7	0.644	95 235.1	0.635	2,5/2
	95 237.1	0.630	95 242.9	0.614	1&3,5/2
	95 273.1	0.700	95 285.7	0.667	2,7/2
			95 289.7	0.657	3,7/2
	Overlap with d state		95 310.0	0.603	3,7/2
	not obs.		95 358.0	0.642	3,9/2
$n=10$	not obs.		95 479.8	0.674	1,1/2
	95 494.1	0.621	95 492.0	0.629	1,1/2
	95 514.1	0.647	95 510.5	0.661	1,3/2
	95 519.1	0.629	95 519.1	0.629	2,3/2

TABLE II. (*Continued.*)

	$S(0)$ $J''=2$ (+)				
	E_{obs} (cm^{-1})	μ_{obs}	E_{theory} (cm^{-1})	μ_{theory}	Assignment[a] J',J^+
	95 522.1	0.617	95 523.3	0.613	1,3/2
	95 546.1	0.658	95 544.3	0.664	2,5/2
	95 555.1	0.624	95 552.5	0.634	1&2,5/2
	Overlap with *d* state				
	not obs.		95 558.9	0.610	3,5/2
	Overlap with *d* state		95 605.8	0.669	2,7/2
	Overlap with *d* state		95 609.6	0.655	3,7/2
	Overlap with *d* state		95 623.6	0.603	3,7/2
	not obs.		95 674.0	0.648	3,9/2
s-Rydberg complex					
$n=7$					
	not obs.		94 446.3	0.089	1,1/2
	94 477.1	0.074	94 471.0	0.083	2,3/2
			94 480.8	0.068	1,3/2
	94 521.7	0.074	94 515.9	0.083	3,5/2
			94 522.0	0.074	2,5/2
	not obs.		94 571.1	0.073	3,7/2
$n=8$					
	not obs.		94 992.5	0.084	1,1/2
	95 024.7	0.058	95 017.5	0.074	1&2,3/2
	95 065.0	0.069	95 061.3	0.077	2,5/2
	not obs.		95 110.2	0.076	3,7/2
$n=9$					
	95 366.1	0.075	95 364.5	0.080	1,1/2
	95 386.2	0.077	95 386.3	0.077	1&2,3/2
	not obs.		95 430.6	0.079	2&3,5/2
	not obs.		95 479.7	0.077	3,7/2
$n=10$					
	95 631.1	0.068	95 629.2	0.077	1,1/2
	95 648.1	0.086	95 649.9	0.078	1&2,3/2
	Overlap with *d* state				
	95 698.1	0.063	95 694.3	0.080	2&3,5/2

[a]See the text for explanation.
[b]See the text for explanation.

is comparable to that of the *d* series, an observation which requires larger transition moments than calculated by *ab initio* methods (see Table V). The *f* states were the most easily identified and assigned series of the Rydberg states. The lines are intense and quite narrow (FWHM ≈ 2.5 cm^{-1}). Moreover, the splitting between the various *P*, *Q*, and *R* branches at $n=7$ is approximately 6 cm^{-1} and drops to ≈ 2 cm^{-1} at $n=10$, in agreement with the requirement that it should vanish as *n* approaches infinity. The *f* states are a clear example of almost Hund's case (e) coupling. The peaks are separated by approximately the ionic rotational spacing indicating that the Rydberg electron is essentially decoupled from the molecular axis. This is not so apparent for the *s*, *p*, and *d* states, since for these states the Hund's case coupling is more of an intermediate nature. The *f* states have not been analyzed using the full MQDT treatment but, instead, their positions and intensities have been calculated using a simple diagonalization procedure which did not include any interactions with the continuum or other Rydberg series. In this procedure a matrix is constructed for each *J* value on the basis of the different states of an *nl* complex with matrix elements expressed in Hund's case (e)[7] and subsequently diagonalized. This method has already been applied successfully to the *nf* complexes of CO_2.[21] Very satisfactory results could be obtained by this procedure, but when the MQDT was performed the maximum intensities and widths of the peaks were misrepresented. This can be attributed to the fact that the widths of *f*-state resonances are very small. In the calculation these widths derive from the differences between the quantum defects of singlet and triplet states. Because the Fano index, *q*, is proportional to $1/\Gamma$ (Γ is the width)[5] and the intensity maxima of the resonances are proportional to q^2, a comparison of the theoretical spectrum with the experimental one is consequently very unreliable. It should be noted, however, that although maximum intensities in the two spectra cannot be compared in the present approach, integrated intensities can be, since these are equal in the MQDT and diagonalization calculations. Using diagonalization is equivalent to assuming a width equal to zero. This can be justified since the *f* states interact very weakly with the

TABLE III. Assignment of spin–orbit autoionizing Rydberg series via the $R(1)$ transition of the $F\ ^1\Delta_2$ Rydberg state of HBr together with results of corresponding MQDT calculations using the rotational ionic thresholds reported in Table I and the fitted parameters given in Tables IV and V.

	$R(1)$ $J''=2$ $(-)$				
	E_{obs} (cm^{-1})	μ_{obs}	E_{theory} (cm^{-1})	μ_{theory}	Assignment[a] J', J^+
f-Rydberg complex[b]					
$n=7$					
	94 479.0	0.039	94 481.9	0.034	3,1/2
	94 482.9	0.033	94 485.5	0.029	3,1/2
	94 499.6	0.039	94 500.5	0.038	2,3/2
	94 513.1	0.018	94 507.1	0.028	3,3/2
	94 547.0	0.036	94 545.1	0.039	2,5/2
	94 555.2	0.023	94 551.7	0.028	3,5/2
	94 587.4	0.048	94 591.3	0.042	1,7/2
	94 593.6	0.039	94 595.6	0.036	2&3,7/2
	94 600.4	0.028	94 598.5	0.031	2,7/2
	94 605.3	0.021	94 603.1	0.024	3,7/2
	94 667.7	0.049	94 672.9	0.041	2,9/2
	94 678.1	0.033	94 679.9	0.030	3,9/2
	Overlap with *d* state				
	94 682.3	0.027	94 683.1	0.025	2,9/2
$n=8$					
	not obs.		95 014.3	0.034	3,1/2
	95 017.2	0.027	95 016.7	0.028	3,1/2
	95 033.5	0.038	95 033.5	0.038	2,3/2
	95 042.3	0.018	95 037.9	0.028	3,3/2
	95 079.7	0.035	95 078.3	0.038	2,5/2
	95 085.3	0.022	95 082.7	0.028	3,5/2
	95 121.8	0.050	95 125.1	0.043	1,7/2
	95 126.7	0.039	95 128.1	0.036	2&3,7/2
	95 131.3	0.028	95 129.9	0.031	2,7/2
	95 134.6	0.021	95 133.0	0.024	3,7/2
	95 204.8	0.045	95 206.5	0.041	2,9/2
	Overlap with *p* state				
	95 213.3	0.026	95 213.3	0.026	2,9/2
	95 209.3	0.035	95 211.1	0.031	3,9/2
$n=9$					
	95 381.7	0.024	95 380.3	0.028	3,1/2
	95 397.3	0.041	95 398.3	0.038	2,3/2
	95 404.6	0.017	95 401.3	0.028	3,3/2
	95 444.7	0.033	95 443.3	0.038	2,5/2
	95 448.0	0.022	95 446.1	0.029	3,5/2
	95 491.3	0.040	95 490.4	0.043	1,7/2
	Overlap with *p* state		95 492.5	0.036	2,7/2
	95 495.3	0.027	95 493.9	0.031	2,7/2
	Overlap with *d* state				
	95 498.3	0.017	95 496.0	0.024	3,7/2
	95 571.7	0.041	95 571.7	0.041	2,9/2
	Overlap with *p* state				
	95 574.3	0.032	95 573.8	0.034	3,9/2
$n=10$					
	95 641.1	0.023	95 640.1	0.028	3,1/2
	95 661.3	0.026	95 659.0	0.037	2,3/2
			95 661.1	0.027	3,3/2
d-Rydberg complex					
$n=7$					
	94 296.7	0.337	94 297.5	0.336	3,3/2
	94 301.4	0.331	94 304.9	0.326	2,3/2
	94 335.7	0.331	94 334.5	0.333	3,5/2
	94 355.9	0.304	94 352.8	0.308	2,5/2
	94 373.0	0.366	94 375.1	0.363	3,7/2
	94 424.7	0.296	94 436.3	0.280	3,7/2
		0.380		0.365	3,9/2
$n=8$					
	94 678.0	0.708	94 675.7	0.712	1,1/2
	Overlap with *f* state				

TABLE III. (*Continued*.)

	$R(1)$ $J''=2$ $(-)$				
	E_{obs} (cm^{-1})	μ_{obs}	E_{theory} (cm^{-1})	μ_{theory}	Assignment[a] J',J^+
	94 697.5	0.721	94 698.6	0.719	1,3/2
	not obs.		94 734.6	0.606	2,1/2
	94 903.3	0.330	94 904.7	0.327	3,3/2
	94 909.5	0.388	94 911.7	0.384	2,5/2
	94 941.3	0.323	94 935.3	0.336	3,5/2
	94 962.4	0.279	94 963.7	0.277	2,5/2
	94 972.9	0.387	94 978.1	0.376	2&3,7/2
$n=9$					
	95 158.7	0.674	95 159.8	0.671	1,1/2
	95 186.3	0.672	95 181.4	0.685	1,3/2
	95 316.0	0.308	95 311.6	0.321	3,3/2
	95 330.3	0.369	95 323.1	0.390	2,5/2
	95 346.9	0.320	95 345.4	0.324	3,5/2
	95 372.3	0.429	95 376.6	0.417	2,7/2
	95 382.0	0.401	95 386.5	0.388	3,7/2
$n=10$					
	95 495.3	0.617	95 494.8	0.618	1,1/2
	Overlap with f state				
	95 515.3	0.643	95 514.6	0.645	1,3/2
	Overlap with p state				
	95 545.6	0.421	95 543.7	0.429	3,1/2
	Overlap with p state				
	95 600.0	0.310	95 599.8	0.310	3,3/2
	95 614.6	0.392	95 613.5	0.397	2,5/2
	95 637.1	0.300	95 637.4	0.299	3,5/2
	95 666.3	0.176	95 669.2	0.164	3,5/2
	not obs.		95 676.0	0.398	2,7/2
p-Rydberg complex					
$n=8$					
	94 692.8	0.685	94 692.8	0.685	1,1/2
	94 719.3		94 711.1	0.652	1,1/2
	Broad peak		94 726.3	0.662	1,3/2
	94 750.3	0.619	94 751.2	0.617	2,3/2
	94 759.4	0.684	94 768.2	0.668	1,5/2
	94 775.6	0.655	94 774.4	0.657	2,5/2
	not obs.		94 789.6	0.629	3,5/2
	94 804.9	0.601	94 800.2	0.610	2,5/2
	94 819.3	0.664	94 820.0	0.552	3,7/2
	not obs.		94 836.5	0.632	3,7/2
	94 845.2	0.616	94 841.6	0.623	2,7/2
	94 896.7	0.670	94 899.7	0.664	3,9/2
$n=9$					
	95 158.7	0.679	95 158.6	0.679	1,1/2
	95 175.0	0.636	95 169.3	0.651	1,1/2
	95 190.6	0.650	95 185.1	0.665	1,3/2
	95 204.8	0.612	95 203.5	0.616	2,3/2
	Overlap with f state				
	95 221.2	0.568	95 228.0	0.549	2,3/2
	95 230.5	0.663	95 232.8	0.657	2,5/2
	not obs.		95 243.3	0.629	3,5/2
	95 254.6	0.599	95 252.1	0.606	2,5/2
	not obs.		95 279.3	0.663	3,7/2
	95 297.2	0.615	95 290.2	0.634	2,7/2
	not obs.		95 358.8	0.666	3,9/2
$n=10$					
	not obs.		95 481.5	0.675	1,1/2
	95 491.3	0.639	95 488.2	0.651	1,1/2
	Overlap with f state				
	95 509.2	0.650	95 504.9	0.666	1,3/2
	95 515.3	0.627	95 511.8	0.641	1,3/2
	Overlap with d state				
	95 522.9	0.599	95 519.3	0.612	2,3/2

TABLE III. (*Continued*.)

	$R(1)$ $J''=2$ $(-)$				
	E_{obs} (cm^{-1})	μ_{obs}	E_{theory} (cm^{-1})	μ_{theory}	Assignment[a] J',J^+
	95 545.6	0.682	95 548.2	0.672	1,5/2
	95 553.0	0.655	95 552.2	0.658	2,5/2
	not obs.		95 559.6	0.630	3,5/2
	95 571.7	0.584	95 566.5	0.604	2,5/2
	Overlap with f state				
	Overlap with d state		95 599.1	0.664	3,7/2
	95 606.7	0.636	95 605.3	0.641	2&3,7/2
	not obs.		95 678.7	0.668	3,9/2
s-Rydberg complex					
$n=7$					
	not obs.		94 446.3	0.086	1,1/2
	94 478.3	0.078	94 473.4	0.085	2,3/2
			94 483.0	0.071	1,3/2
	94 523.7	0.062	94 517.6	0.071	2,5/2
	not obs.		94 578.1	0.075	3,7/2
$n=8$					
	not obs.		94 991.8	0.081	1,1/2
	95 022.3	0.073	95 020.4	0.077	1&2,3/2
	95 070.6	0.042	95 056.1	0.075	2,5/2
	not obs.		95 118.0	0.077	3,7/2
$n=9$					
	not obs.		95 363.2	0.077	1,1/2
	95 396.4	0.057	95 389.7	0.079	1&2,3/2
	not obs.		95 425.0	0.077	2&3,5/2
	not obs.		95 487.4	0.079	3,7/2
$n=10$					
	95 631.3	0.058	95 627.6	0.075	1,1/2
	Overlap with d state				
	95 650.3	0.094	95 653.6	0.079	1&2,3/2
	not obs.		95 688.5	0.079	2&3,5/2

[a]See the text for explanation.
[b]See the text for explanation.

$^2\Pi_{3/2}$ continuum, and hence behave as though they are below the lowest ionization limit. Because the f states have been calculated using the diagonalization approach, we are unable to obtain their absolute transition moments directly. However, some of the $J'=1$ d states are very narrow and their intensities calculated using the diagonalization method can therefore be directly compared to those of the f states. Such a comparison allows for the determination of the absolute f transition moments (see Table V).

Figures 3 and 4 show good agreement between the MQDT based predicted spectra and the experimental ones. In fact, in comparison with similar analyses of autoionizing states in other hydrogen halides such as HI[2] and HCl[3,4] the present analysis shows a considerably better agreement. The fact that there still remain some discrepancies should come as no surprise, since a number of factors that might be of influence have not been dealt with in the present model. It is known that l is never a good quantum number in molecules, and there will always be a certain degree of l mixing present which could cause some slight changes in positions and intensities of the calculated lines. Another problem might arise from perturbations from high vibrational levels of the $\cdots\sigma^1\pi^4\sigma^*$ $V\ ^1\Sigma^+$ valence state. A preliminary asymptotic energy value obtained for the formation of ion pairs, $H^+ + Br^-$ ($\approx$14 eV),[22] reveals that the $V\ ^1\Sigma^+$ state has vibrational interlopers covering the whole of the spin–orbit region. Although there is no direct transition moment to the $V\ ^1\Sigma^+$ vibrational states, these states might mix into the final state wave functions. Another source of perturbations can also derive from vibrationally excited interlopers built upon the $^2\Pi_{3/2}$ and $^2\Pi_{1/2}$ ionic cores. Also these states might be mixed into the final state wave functions.

C. Comparison with one-photon excitation spectrum

Recently a high resolution one-photon excitation spectrum of HBr in the spin–orbit autoionization region has been measured.[10] When this spectrum, which we will refer to as the X spectrum, is compared to our spectrum via the $S(0)$ transition of the $F\ ^1\Delta_2$ state, referred to as the F spectrum, we find that there is virtually no resemblance between them. This is not so peculiar as it may seem for the following reasons. First, the transition moments are different for both types of spectra, since the allowed one-photon transitions from the $X\ ^1\Sigma_0^+$ state are to $^1\Pi_1$ and $^1\ \Sigma_0^+$ states, while from the $F\ ^1\Delta_2$ state they are to $^1\Pi_1$, $^1\Delta_2$, and $^1\Phi_3$ states. It is

TABLE IV. Quantum defects obtained from the fit of MQDT predicted autoionization spectra via the $F\ ^1\Delta_2$ Rydberg state of HBr to the present experimental spectra. For comparison, the values from an *ab initio* calculation (Ref. 13), which have been used as the initial values in the fit, have been given in parentheses.

	$l=0$	$l=1$		$l=2$			$l=3$			
	$s\sigma$	$p\sigma$	$p\pi$	$d\sigma$	$d\pi$	$d\delta$	$f\sigma$	$f\pi$	$f\delta$	$f\phi$
$^1\Pi$	0.001	0.615		0.770			0.048			
	(−0.021)	(0.533)		(0.643)			(0.023)			
$^3\Pi$	0.105	0.715		0.805			0.059			
	(0.047)	(0.566)		(0.695)			(0.022)			
$^1\Sigma^+$			0.500		0.100			0.010		
			(0.387)		(0.078)			(0.032)		
$^3\Sigma^-$			0.600		0.185			0.013		
			(0.481)		(0.253)			(−0.012)		
$^1\Sigma^-$			0.600		0.185			0.013		
			(0.481)		(0.253)			(−0.012)		
$^3\Sigma^+$			0.700		0.330			0.020		
$^1\Delta$			0.570		0.290			0.023		
$^3\Delta$			0.630		0.405			0.035		
$^1\Pi$						0.145			0.031	
						(−0.005)				
$^3\Pi$						0.305			0.042	
						(0.408)				
$^1\Phi$						0.205			0.015	
$^3\Phi$						0.330			0.036	
$^1\Delta$										0.011
$^3\Delta$										0.020
$^3\Gamma$										0.020

important to note that the transition to a $[^2\Pi]l\delta\ ^1\Pi_1$ state is only possible from the $X\ ^1\Sigma_0^+$ and not from the $F\ ^1\Delta_2$ state.[16] Second, if we assume that in the X spectrum the lowest rotational state, $J''=0$, is predominantly populated, then only transitions via the R branch are allowed, i.e., $J'=1$ final states are solely accessible. The $J'=1$ states in our F spectrum correspond to the P branch which is weaker than the Q and R branches. Hence, we anticipate the autoionization spectra to appear very different. Only the $J'=1$ Rydberg states are common to both spectra, but they will have very different intensities, strong in the X and weak in the F spectrum.

Despite these dissimilarities, one should be able to simulate both spectra using a common set of quantum defects. In order to verify our assignments we have therefore also performed MQDT calculations of the autoionization spectra for excitation from the $X\ ^1\Sigma_0^+$ state using the quantum defects given in Table IV and transition moments derived in Ref. 13 (not shown). Apart from such a verification this simulation is expected to also enable us to determine more accurately the quantum defects of those Hund's case (a) basis states that carry no transition moment in the corresponding F spectrum, which would be insensitive to changes in these quantum defects. From the calculations we find good correspondence between simulated and experimental spectra, especially for the d states. However, unlike in the F spectrum, no experimental evidence has been found for the presence of f states. Furthermore, we could not unambiguously identify the p states. Some indications for these states were observed, but it seems that the transitions to these states are too weak to allow a solid assignment. The observation that p and f states are weak or absent would be in agreement with the fact that the outer electron of the $X\ ^1\Sigma_0^+$ state has predominantly p character, resulting in s and d final states after one-photon absorption. Further support derives from a one-photon ZEKE-PFI study where no indication for odd partial waves was found.[9] Nevertheless, the X spectrum shows that only s- and d-Rydberg states are not sufficient to characterize the whole spectrum, since a plethora of other resonances of smaller intensity were observed. To account for these numerous peaks the following explanations come to mind. From the ground state there is significant Franck–Condon overlap with the $v'=1$ vibrational interlopers of Rydberg states converging to either the $^2\Pi_{3/2}$ or $^2\Pi_{1/2}$ ionic states, unlike what is expected for a Rydberg–Rydberg transition. Moreover, the HBr beam temperature, which was reported to be 8.5 K[10] would imply a significant population of the $J''=1$ rotational level of the $X\ ^1\Sigma_0^+$ state (≈16%). This means that $J'=0$, 1,

TABLE V. Transition moments (a.u.) obtained from the fit of MQDT predicted autoionization spectra via the $F\ ^1\Delta_2$ Rydberg state of HBr to the present experimental spectra. For comparison, the transition moments from an *ab initio* calculation (Ref. 16) are indicated in parentheses.

	l	0	1	2	3[a]
	λ				
$F\ ^1\Delta-{}^1\Pi$	0	0.700	1.140	−0.600	0.240
		(0.835)	(0.316)	(−0.666)	(0.000)
$F\ ^1\Delta-{}^1\Delta$	1		−0.750	0.728	0.720
			(−0.281)	(0.728)	(0.095)
$F\ ^1\Delta-{}^1\Phi$	2			1.118	0.540
				(1.118)	(0.071)

[a]See the text for explanation.

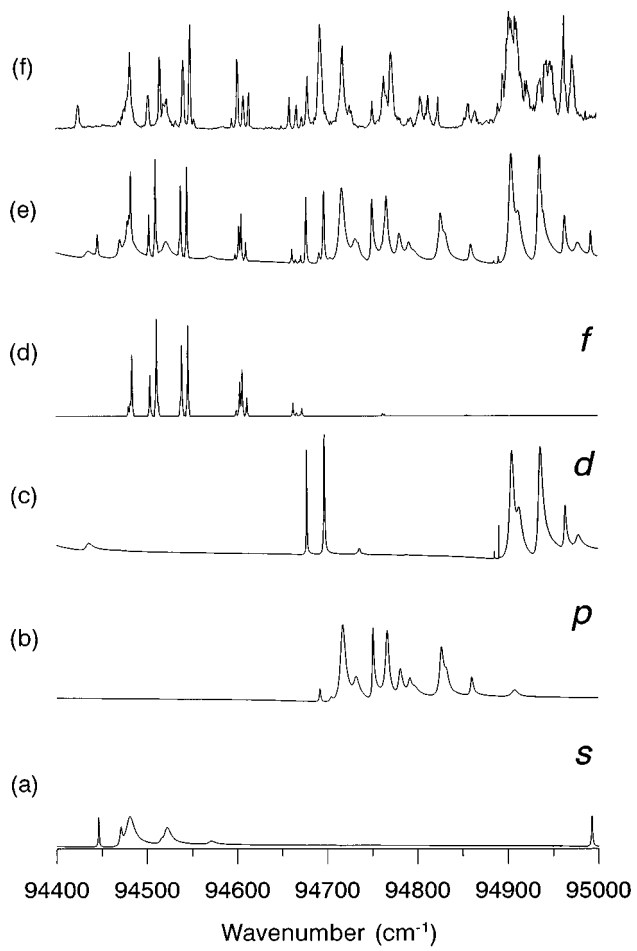

FIG. 3. MQDT simulation of the spin–orbit autoionization spectra via the $S(0)$ $F\ ^1\Delta_2$ rotational transition compared to the experimental spectrum. The individual Rydberg series are displayed in (a)–(d), which correspond to simulations of the s, p, d, and f states, respectively. In (e) the simulation including all Rydberg series convoluted with a 1 cm^{-1} Gaussian line form is displayed, while in (f) the corresponding part of the experimental spectrum is shown.

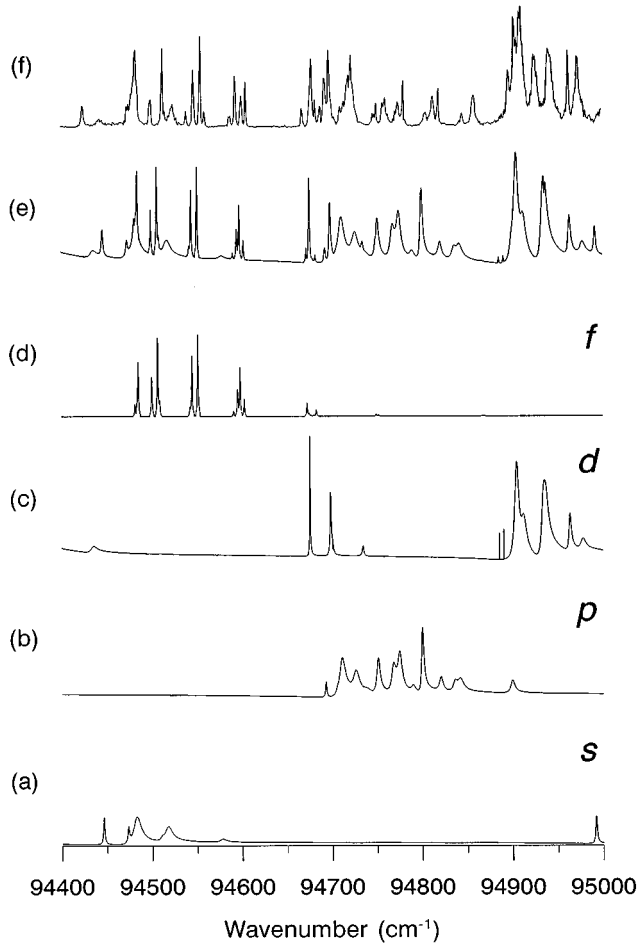

FIG. 4. MQDT simulation of the spin–orbit autoionization spectra via the $R(1)$ $F\ ^1\Delta_2$ rotational transition compared to the experimental spectrum. The individual Rydberg series are displayed in (a)–(d), which correspond to simulations of the s, p, d, and f states, respectively. In (e) the simulation including all Rydberg series convoluted with a 1 cm^{-1} Gaussian line form is displayed, while in (f) the corresponding part of the experimental spectrum is shown.

and 2 final states are accessible as well from this level. Finally, as with the F spectrum, l mixing, and $V\ ^1\Sigma^+$ valence state contributions will certainly perturb the observed autoionizing states but, in addition, the $V\ ^1\Sigma^+$ rovibronic levels would be directly accessible from the ground state. All in all the autoionization spectrum from the $X\ ^1\Sigma_0^+$ state is complicated by these additional factors, thereby inhibiting a more complete analysis.

Apart from the different range of J' values accessible in the two experiments, it should be recognized that identical states are excited in both experiments. This implies that the differences observed in the intensities of the various l states when exciting from the $F\ ^1\Delta_2$ or the $X\ ^1\Sigma_0^+$ states must necessarily derive from the differences in the angular momentum composition of the electron which is excited, i.e., the $4p\pi$ electron in case of excitation from the $X\ ^1\Sigma_0^+$ and the $5p\pi$ electron in case of excitation from the $F\ ^1\Delta_2$ Rydberg state. We therefore conclude that higher angular momenta contribute significantly more to the $5p\pi$ orbital than to the $4p\pi$ orbital.

IV. CONCLUSIONS

In this paper we have investigated extensively rotationally resolved spin–orbit autoionizing Rydberg states excited in a double resonant two-color $(2+1')$ excitation process via the $F\ ^1\Delta_2$ $(v''=0)$ Rydberg state. MQDT calculations have been found to be mandatory for a proper analysis of the spectra, which show Rydberg series with l ranging from 0 to 3. For the range of principal quantum numbers studied here $(n=7$ to 10) these states are found to be described as intermediate between Hund's case (c) and case (e) coupling, with almost pure Hund's case (e) coupling for $l=3$ Rydberg states. Interestingly, the presence of odd (p and f) Rydberg series is underestimated by *ab initio* calculations, although it is in excellent agreement with the results of our previous ZEKE-PFI studies in which odd partial waves were found to be significant contributors to the ionization dynamics. The availability of accurate ionization thresholds and the lower density of states in the present spectra has been shown to

lead to a considerable improvement between experiment and theory as compared to similar studies on other hydrogen halides.

ACKNOWLEDGMENTS

The group at the University of Amsterdam gratefully acknowledges the Netherlands Organization for Scientific Research (N.W.O.) for equipment grants and for financial support. N.P.L.W. thanks N.W.O. for a bursary for a stay at the Université de Paris-Sud. Calculations performed by H.L.B. have used the French National Computer (CNUSC).

[1] K. S. Haber, E. Patsilinakou, Y. Jiang, and E. R. Grant, J. Chem. Phys. **94**, 3429 (1991).
[2] A. Mank, M. Drescher, T. Huth-Fehre, N. Böwering, U. Heinzmann, and H. Lefebvre-Brion, J. Chem. Phys. **95**, 1676 (1991).
[3] Y.-F. Zhu, E. R. Grant, and H. Lefebvre-Brion, J. Chem. Phys. **99**, 2287 (1993).
[4] M. Drescher, A. Brockhinke, N. Böwering, U. Heinzmann, and H. Lefebvre-Brion, J. Chem. Phys. **99**, 2300 (1993).
[5] H. Lefebvre-Brion, A. Giusti-Suzor, and G. Raseev, J. Chem. Phys. **83**, 1557 (1985).
[6] H. Lefebvre-Brion, J. Chem. Phys. **93**, 5898 (1990).
[7] H. Lefebvre-Brion, in *High Resolution Laser Photoionization and Photoelectron Studies*, edited by I. Powis (Wiley, New York, 1995), p. 171.
[8] N. P. L. Wales, W. J. Buma, C. A. de Lange, H. Lefebvre-Brion, K. Wang, and V. McKoy, J. Chem. Phys. **104**, 4911 (1996).
[9] R. Irrgang, M. Drescher, F. Gierschner, M. Spieweck, and U. Heinzmann, J. Elect. Spectrosc. Relat. Phenom. **80**, 5 (1996).
[10] R. Irrgang, N. Böwering, M. Drescher, M. Spieweck, and U. Heinzmann, J. Chem. Phys. **104**, 8699 (1996).
[11] *CRC Handbook of Chemistry and Physics*, 66th ed., edited by R. C. Weast (CRC, Boca Raton, 1985–1986), p. E-259.
[12] R. Callaghan and R. J. Gordon, J. Chem. Phys. **93**, 4624 (1990).
[13] H. Lefebvre-Brion, P. M. Dehmer, and W. A. Chupka, J. Chem. Phys. **85**, 45 (1986).
[14] K. Wang and V. McKoy, J. Chem. Phys. **95**, 7872 (1991).
[15] K. G. Lubic, D. Ray, D. C. Hovde, L. Veseth, and R. J. Saykally, J. Mol. Spectrosc. **134**, 21 (1989).
[16] H. Lefebvre-Brion, Chem. Phys. Lett. **171**, 377 (1990).
[17] Y.-F. Zhu, E. R. Grant, K. Wang, V. McKoy, and H. Lefebvre-Brion, J. Chem. Phys. **100**, 8633 (1994).
[18] M. L. Ginter and S. G. Tilford, J. Mol. Spectrosc. **34**, 206 (1970).
[19] M. L. Ginter and S. G. Tilford, J. Mol. Spectrosc. **37**, 159 (1971).
[20] D. S. Ginter, M. L. Ginter, and S. G. Tilford, J. Mol. Spectrosc. **90**, 152 (1981).
[21] C. Cossart-Magos, H. Lefebvre-Brion, and M. Jungen, Mol. Phys. **85**, 821 (1995).
[22] A. J. Yencha, A. Hopkirk, J. R. Grover, B.-M. Cheng, H. Lefebvre-Brion, and F. Keller, J. Chem. Phys. **103**, 2882 (1995).